The Planetary Science Journal, 2:189 (11pp), 2021 October https://doi.org/10.3847/PSJ/ac1d53


# Lunar Surface Composition Constraints from Maturity-corrected Far-ultraviolet Reflectance Maps

Benjamin D. Byron[1,2,5], Kurt D. Retherford[2,1], Elizabeth Czajka[1,2], Joshua T. S. Cahill[3], Amanda R. Hendrix[4], and Thomas K. Greathouse[2]

[1] Department of Physics and Astronomy, University of Texas at San Antonio, 1 UTSA Circle, San Antonio, TX 78249, USA; benjamin.d.byron@jpl.nasa.gov
[2] Space Science and Engineering Department, Southwest Research Institute, 6220 Culebra Road, San Antonio, TX 78238, USA
[3] Johns Hopkins University Applied Physics Laboratory, 11100 Johns Hopkins Road, Laurel, MD 20723, USA
[4] Planetary Science Institute, 1700 East Fort Lowell, Suite 106, Tucson, AZ 85719, USA
*Received 2021 May 12; revised 2021 August 5; accepted 2021 August 10; published 2021 September 13*

## Abstract

Far-ultraviolet (FUV) observations by the Lunar Reconnaissance Orbiter Lyman Alpha Mapping Project (LAMP) have shown that the lunar surface reflectance in the ultraviolet is sensitive to changes in both composition and maturity at wavelengths >170 nm. This can lead to uncertainties in the interpretation of features that appear in maps created using LAMP data from this wavelength range. Here we utilize a correction based on the optical maturity parameter to remove large-scale immaturity features from LAMP spectral slope and band ratio maps. After performing the correction, the LAMP maps more accurately represent the FUV lunar surface in the context of composition. Corrected LAMP maps show good correlation with lunar FeO, plagioclase, and bulk silicate abundance maps for moderate- to high-iron regions, indicating a sensitivity in the LAMP data to differences in mineral composition in those regions. These maps represent a unique view into a relatively unexplored region of the spectrum and showcase the ability to perform compositional mapping and mineral identification using FUV remote-sensing measurements.

*Unified Astronomy Thesaurus concepts:* The Moon (1692); Lunar composition (948); Lunar science (972)

## 1. Introduction

Recent studies utilizing data from the Lunar Reconnaissance Orbiter (LRO) Lyman Alpha Mapping Project (LAMP) have characterized the sensitivity of far-ultraviolet (FUV) surface reflectance to changes in lunar regolith surface maturity due to space weathering (Hendrix et al. 2012, 2016; Byron et al. 2019, 2020a; Cahill et al. 2019). Space weathering processes (e.g., solar wind and micrometeoroid bombardment) act to alter the regolith grains at the lunar surface, causing changes in spectral properties that can be observed by instruments with sensing capabilities ranging from the UV to the thermal infrared (IR) (Pieters et al. 2000; Lucey et al. 2017). At visible to near-IR wavelengths, space weathering acts to redden (i.e., increase slope with wavelength) the spectral slope and darken the reflectance spectrum (Noble et al. 2007). In the FUV (100–200 nm), however, the relative decrease in albedo is limited to wavelengths >∼170 nm, and the spectral slope is instead decreased by weathering, and only for highlands material (Hendrix et al. 2016). Immature regions of the lunar highlands therefore have redder spectral slopes in the FUV, and over time, the spectral slope >170 nm decreases at these regions with the accumulation of additional weathering exposure. This bluing is caused by a degradation of the UV silicate absorption edge through the addition of opaque submicroscopic iron (SMFe) inclusions (a by-product of space weathering) to the transparent host grain (Hendrix & Vilas 2006; Hendrix et al. 2016).

At wavelengths <170 nm, the lunar surface is spectrally blue, and the spectral slope is little affected by changes in regolith maturity (Hendrix et al. 2016; Byron et al. 2020b). This is a result of lunar host minerals being increasingly opaque shortward of ∼170 nm, meaning that the ability of light to penetrate into the grain far enough to interact with SMFe inclusions in the matrix gradually lessens. While the spectral slope is not affected by regolith maturity at these shorter wavelengths, the overall albedo is (i.e., immature features such as crater rays have a lower albedo than mature regolith at Ly$\alpha$; Cahill et al. 2019). This is because space weathering can affect the FUV reflectance in ways other than SMFe accumulation on regolith grains, e.g., by increasing the index of refraction of individual grains through amorphization or altering the microphysical structure of the regolith.

LAMP is also sensitive to regolith composition at similar wavelengths to those that are affected by regolith maturity (i.e., characteristic mineral absorption bands can also affect the reflectance and/or spectral slope as measured by LAMP). Highlands material, for example, displays a redder spectral slope than the maria >170 nm (Hendrix et al. 2016). To illustrate this, we present a 170–187 nm spectral slope map (Byron et al. 2020b) and an off-band (155–190 nm)/on-band (130–155 nm) albedo ratio (off/on) map (Byron et al. 2020a) in Figure 1, alongside a map of the optical maturity (OMAT) parameter (see Section 2 for a description of these parameters). We see that both composition and maturity features are present in these LAMP maps. Because the LAMP parameters are affected by both regolith maturity and mineral composition, efforts to perform compositional analyses with LAMP may become complicated by the effects of regolith maturity.

In this work, we perform a correction to the global FUV spectral slope and off-band/on-band ratio maps in order to mitigate the effects of regolith maturity. This approach has

[5] Present Location: Jet Propulsion Laboratory, California Institute of Technology, 4800 Oak Grove Drive, Pasadena, CA 91109, USA.

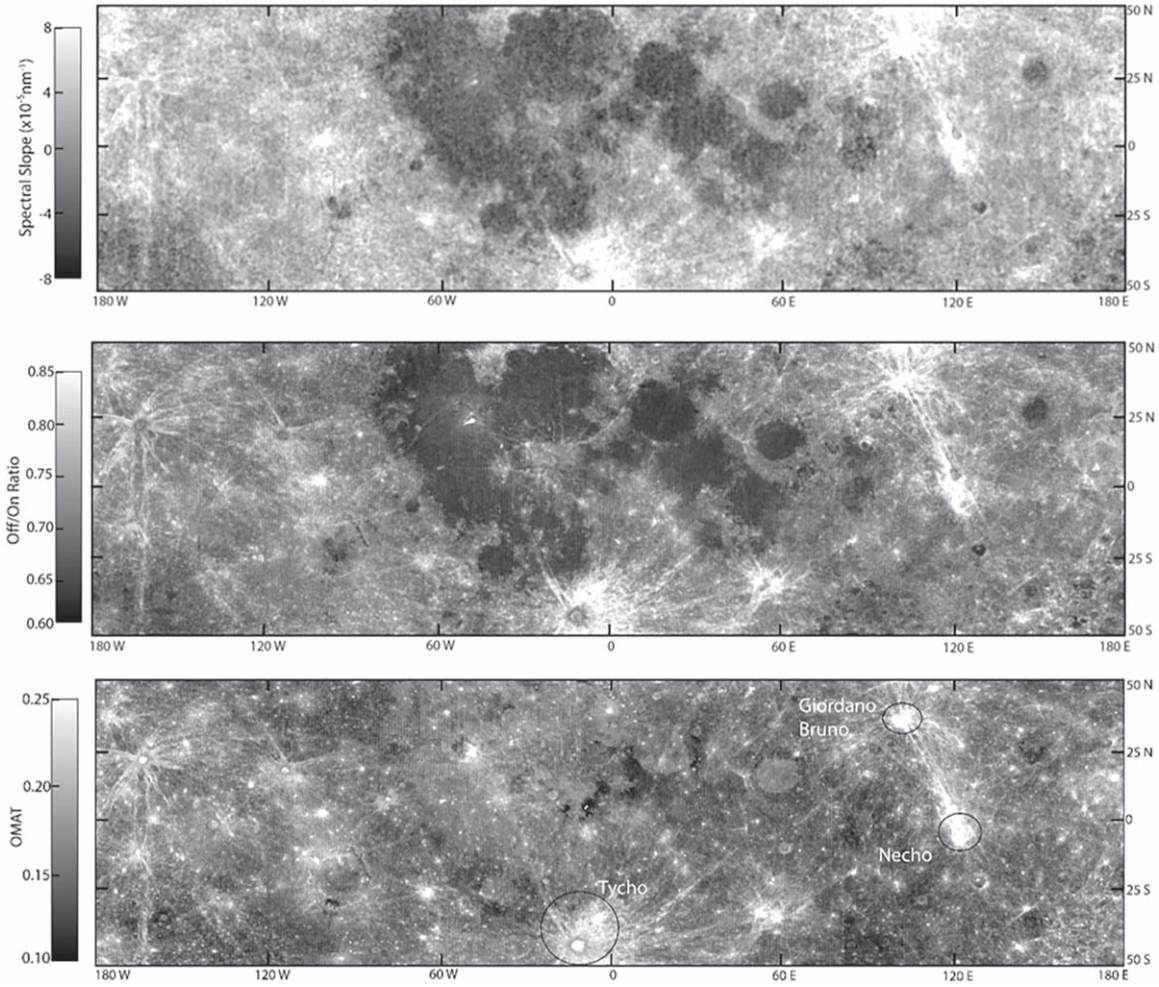


**Figure 1.** LAMP parameter maps before applying the OMAT correction. (Top) LAMP 170–187 nm spectral slope map, (middle) LAMP off/on ratio map, and (bottom) OMAT parameter map, all covering ±50° latitude. Both LAMP parameter maps display features related to regolith maturity (e.g., crater rays) and composition (maria/highlands). Rayed craters Tycho, Giordano Bruno, and Necho are labeled in the OMAT map.

previously been applied to lunar remote-sensing data in the form of a correction to the global Christiansen feature (CF) position map from the LRO Diviner Lunar Radiometer instrument (Lucey et al. 2017). Here we employ a similar method and present corrected LAMP maps where the effects of maturity are mitigated, enabling more accurate compositional studies to be performed with LAMP in the future.

## 2. Methods

### 2.1. The LAMP Instrument and Data

LAMP is an imaging spectrograph on board LRO with a spectral bandpass covering 57–196 nm (Gladstone et al. 2010). The LRO is nominally nadir-pointed and orbited the Moon in a 50 km circular orbit during the primary mission phase (2009 October–2011 December). In 2011 December, LRO changed to an elliptical orbit that enabled up to ∼250 m spatial resolution at the South Pole while reducing spatial resolution at the North Pole to ∼2 km. LAMP collects data during both lunar night and day, measuring surface-reflected starlight and Ly$\alpha$ sky glow at night and surface-reflected sunlight during the day. In 2016 October, LAMP entered a new operating mode in which a fail-safe aperture door was opened in order to increase throughput of light to the detector (Davis et al. 2017). However, to keep from complicating our analysis, we use only dayside data taken before the fail-safe door opening in this study.

The off/on ratio maps we analyzed in this study were made by dividing global maps covering two averaged broad-wavelength bands (on band: 130–155 nm; off band: 155–190 nm) that were defined by the LAMP Global Mapper tool (Gladstone et al. 2012). The on and off bands were originally defined to be most useful in the detection of water ice at the lunar poles using nighttime data. After application to nonpolar daytime data, the ratio of these bands was found to be sensitive to space weathering effects as well (Hendrix et al. 2016; Byron et al. 2020a). The off/on ratio map used in this study has a spatial resolution of 32 pixels per degree (ppd).

The spectral slope maps analyzed in this work were made using another mapping tool developed by the LAMP team called the Spectral Mapper (Mandt et al. 2016; Liu et al. 2018; Byron et al. 2019, 2020b). The Spectral Mapper is primarily used to study smaller regions of the lunar surface at high spectral resolution, as it creates 3D data cube maps with 2 nm spectral resolution. In order to create the global (±50° latitude) coverage map presented in Figure 1, we mosaicked together smaller reflectance maps (each covering 20° longitude and ±50° latitude) into a final 3D global map (with the third dimension being the spectral dimension) containing all nadir-pointing dayside data from the start of the primary mission

phase (2009 October) through 2016 October. The reflectance product of the final map is a radiance factor (I/F) that has been corrected for observational geometry effects and normalized to a 30° phase angle. The Hapke photometric parameters $w$ and $b$ (where $w$ is the single scattering albedo and $b$ is the asymmetry factor) used by the correction were derived from model fits to LAMP data. In the FUV, the derived single scattering albedo $w$ is generally blue-sloped and decreases from ∼0.09 at 134 nm to ∼0.06 at 184 nm, and the asymmetry factor $b$ is roughly constant at −0.5 across the same wavelength range for both maria and highlands regions (Liu et al. 2018).

From this final dayside reflectance map, the slope of the reflectance spectrum between 170 and 187 nm was calculated for each pixel. The 170 nm minimum wavelength was chosen because it was found to be the point at which regions of different maturity and/or composition begin to consistently display variability in spectral slope (shortward of 170 nm, the entire lunar surface has a generally negative slope; Byron et al. 2020b). At wavelengths >187 nm, the LAMP microchannel plate detector experiences increased background counts that are difficult to properly remove from the LAMP daytime data, and those data were thus excluded from this study. Therefore, the region from 170 to 187 nm was found to be the optimal wavelength range for analyzing regolith maturity and composition in this study. The final spectral slope product is a 2D map with a spatial resolution of 10 ppd.

### 2.2. The Maturity Correction

In order to deconvolve the effects of maturity and composition in our LAMP spectral slope and off/on ratio maps, we followed the method of Lucey et al. (2017) and applied an empirical correction using global maps of OMAT. OMAT is a measure of the degree of space weathering that a location on the surface of the Moon has sustained. As seen in Figure 1, ejecta from young, immature craters have high OMAT, while more mature surfaces have lower OMAT values. The idea behind this correction is that because our spectral slope and off/on ratio parameters depend on both composition and maturity, an independently determined maturity parameter (OMAT) could mitigate the LAMP maps from the larger and most problematic effects of maturity. Similar to the method of Lucey et al. (2017), our determination of success depends on the removal or normalization of large-scale maturity features (such as crater rays) from our spectral slope and ratio maps.

A distinction to note is that we made use of the OMAT maps derived from Kaguya Multiband Imager (MI) data (Lemelin et al. 2016), while Lucey et al. (2017) used OMAT maps created from Clementine data (Lucey et al. 2000) to correct their CF location maps. We chose to use the newer Kaguya OMAT maps because of the improved photometric calibration applied to the Kaguya reflectance data. The Kaguya OMAT map covers ±50° latitude and has a spatial resolution of 512 ppd. In order to perform the correction, we decreased the resolution of the OMAT map to match the respective resolutions of the spectral slope and off/on ratio maps.

The formula for the maturity correction contains a factor to scale the OMAT values and the addition of an offset to determine an adjusted LAMP parameter value:

$$\mathrm{LAMP\_param}_{\mathrm{adjusted}} = \mathrm{LAMP\_param}_{\mathrm{orig}} - (\mathrm{factor} * \mathrm{OMAT}) + \mathrm{offset}. \quad (1)$$

We applied this general formula (modeled after the Lucey et al. 2017 correction) to perform the corrections on the spectral slope and off/on ratio maps. The purpose of the OMAT factor is to get OMAT on the same "scale" as the LAMP parameters so that the subtraction can be performed. Lucey et al. (2017) noted that the OMAT scale factor that best removed the maturity features from the Diviner CF maps was 1.0, by coincidence. The LAMP spectral slope values are on the order of $10^{-5}$, however, while the OMAT values mostly vary between 0.1 and 0.3. Therefore, a scale factor of $\sim 10^{-4}$ would be necessary in order to perform the subtraction of the OMAT features from the spectral slope map. We tested different factors through the process of visual trial and error until the large-scale immaturity features (e.g., large craters and rays) were normalized with the background regolith in the spectral slope map and then repeated the same process for the off/on ratio map.

The next step after determining the scale factor was to determine the offset value. In Lucey et al. (2017), the offset in the correction formula was defined such that the Diviner CF values would be tied to known values determined from laboratory measurements (e.g., setting the Diviner CF for a location on the Moon containing exposed anorthite so that it matches the measured CF location of anorthite under simulated lunar conditions). Because laboratory measurements of lunar minerals are scarce in the FUV (and measurements of the off/on ratio and 170–187 nm spectral slope have not been made for the existing lab spectra), we could not define our offset in the same way as Lucey et al. (2017). Instead, we chose the offset values such that the modes of the histograms (i.e., the most frequent values) for our adjusted maps would equal the modes of the original uncorrected histograms. We chose to do it this way so that, even though these final corrected values would not be tied to specific lab-measured values, the off/on ratio and spectral slope values would be consistent with previously reported values from earlier LAMP studies (Gladstone et al. 2012; Byron et al. 2020a).

The initial maturity corrections that provided the best results when applied to the spectral slope (abbreviated as *ss*) and off/on ratio (abbreviated as *oo*) maps are as follows:

$$ss_{\mathrm{adjusted\_1}} = ss_{\mathrm{orig}} - (8.5 \times 10^{-4} * \mathrm{OMAT}) + 1.4 \times 10^{-4}, \quad (2)$$

$$oo_{\mathrm{adjusted\_1}} = oo_{\mathrm{orig}} - (1.5 * \mathrm{OMAT}) + 0.235. \quad (3)$$

This initial correction removed most of the maturity-related features from the LAMP parameter maps. Increasing the factor values beyond this point led to a slight overcorrection throughout much of the highlands. Some of the youngest and largest crater rays, however, were still somewhat apparent in these corrected maps with slightly higher spectral slope and off/on ratio values than surrounding regions (Figure A2). In order to fully normalize these youngest features in the resulting maps, we performed a separate correction (with slightly higher factor values) on pixels with OMAT >0.2. These pixels represent the most immature regions of the lunar surface, where the initial correction may not have fully removed the crater rays from the spectral slope and off/on ratio maps. The separate corrections that were applied to these pixels are listed below:

$$ss_{\mathrm{adjusted\_2}} = ss_{\mathrm{orig}} - (1.1 \times 10^{-3} * \mathrm{OMAT}) + 1.6 \times 10^{-4}, \quad (4)$$

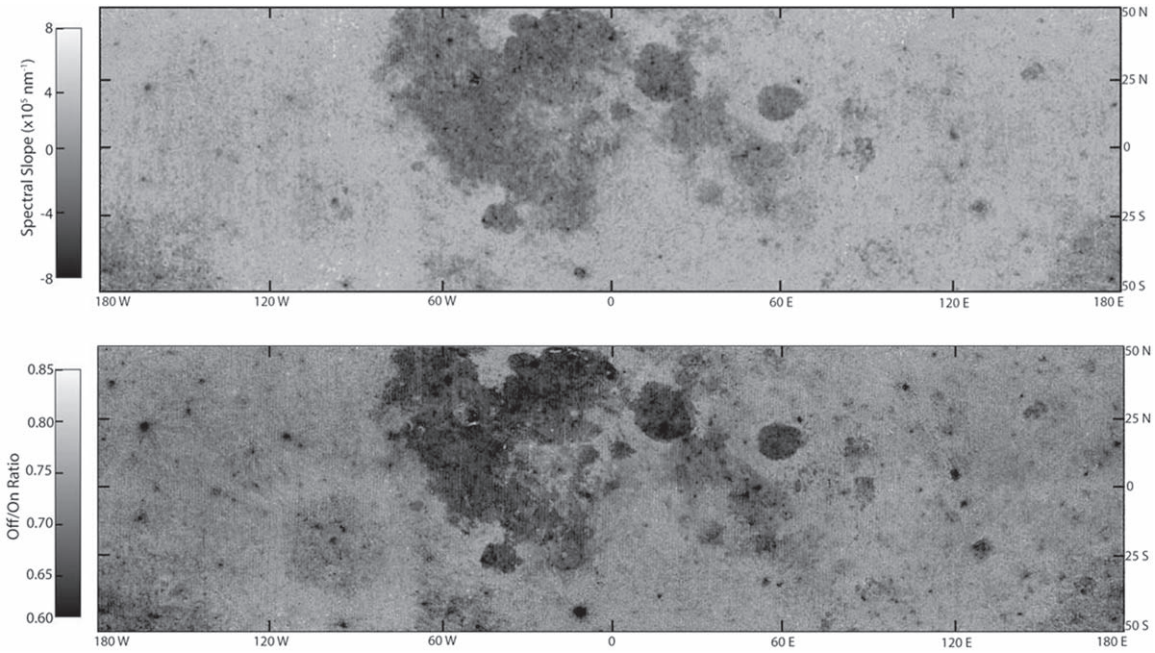


**Figure 2.** LAMP parameter maps after applying Equations (2)–(5). (Top) LAMP 170–187 nm spectral slope map and (bottom) off/on ratio map. Large-scale immaturity features (e.g., crater rays) have been removed from the maps, revealing compositional features. However, artifacts due to overcorrection appear at some locations in the maria.

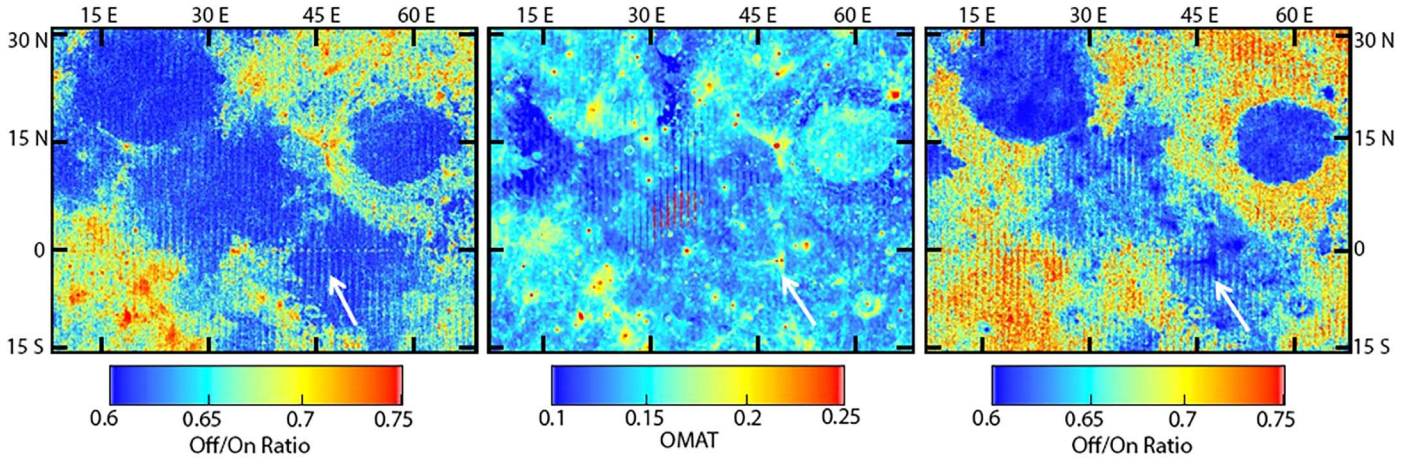


**Figure 3.** Quality of maria region corrections. (Left) Uncorrected off/on ratio map, (middle) OMAT map, and (right) corrected off/on ratio map. White arrows display an artifact resulting from the correction, as further highlighted in Figure 4. The FUV OMAT correction is optimized for highlands ray features but has the potential for additional artifacts in the maria.

$$oo_{\text{adjusted\_2}} = oo_{\text{orig}} - (2 * \text{OMAT}) + 0.305. \quad (5)$$

Figure 2 shows the adjusted spectral slope and off/on ratio maps after applying Equations (2)–(5). Large-scale immaturity features (such as crater rays) have been removed, implying a successful correction. However, as will be explained in the following section, further adjustment is needed.

### 2.3. Artifacts in the Maria

It must be noted that some features appearing in the OMAT map do not appear in the uncorrected spectral slope and off/on ratio maps. For example, ejecta from young craters in the maria that are small enough that they do not excavate underlying feldspathic material display high values in the OMAT map but do not stand out from the background in the original LAMP maps. This discrepancy occurs because of the high opacity of mafic minerals in the FUV (i.e., mafic minerals are entirely surface-scattering in the FUV, and light cannot penetrate far enough into the mineral to interact with space weathering products such as SMFe; Hendrix et al. 2016). Hence, some artifacts appear in the corrected LAMP maps (Figure 3) because in the correction process, we have essentially subtracted maturity-related features that do not appear as clearly in the LAMP maps as they do in the OMAT maps due to the stronger FUV mafic absorption.

One example of such an artifact is found in Mare Fecunditatis, where the ejecta from craters Messier and Messier A appear as anomalously low-ratio features in the corrected off/on ratio map. The ejecta from these craters do not stand out

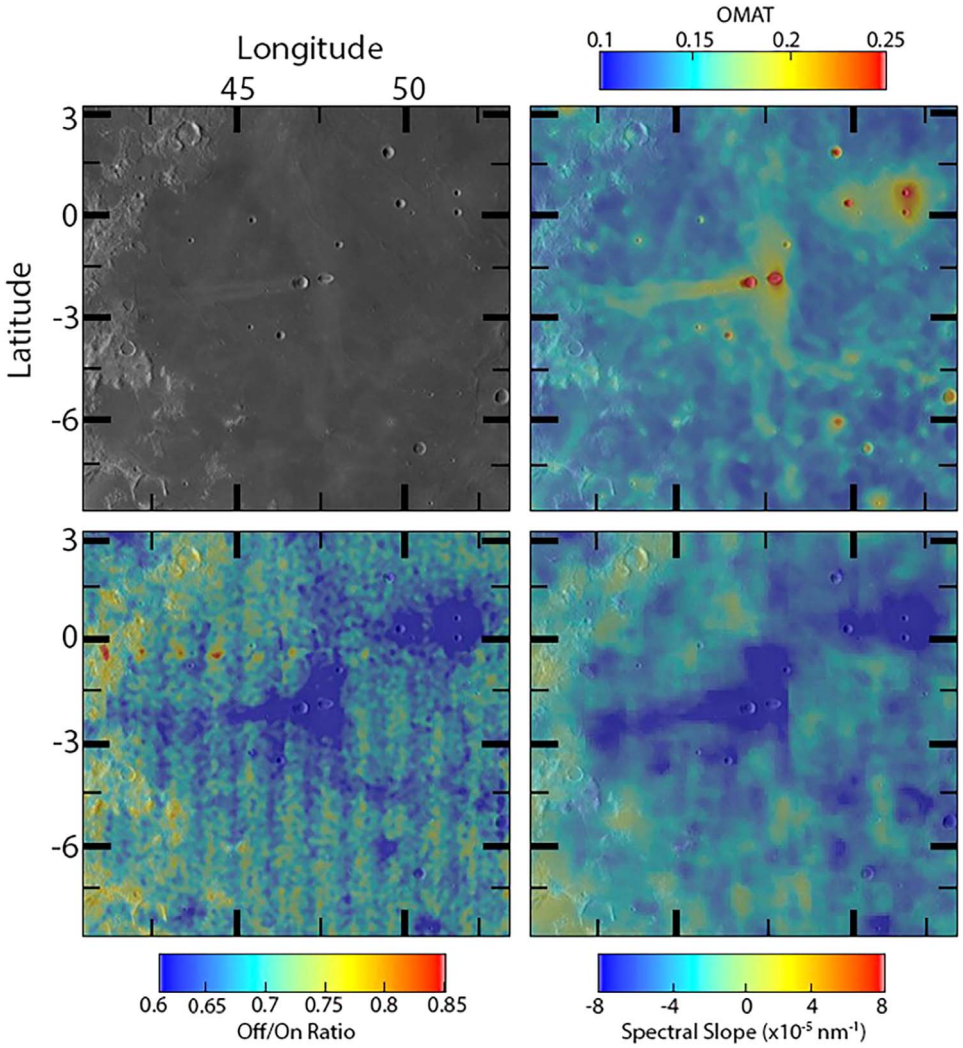


**Figure 4.** Overcorrection in the maria. (Top left) LROC WAC image of Mare Fecunditatis, (top right) OMAT map, (bottom left) corrected off/on ratio map, (bottom right) corrected spectral slope map. The ejecta from fresh craters in the maria (e.g., Messier and Messier A; center of image) are overcorrected in the off/on ratio and spectral slope maps. This occurs because of the high opacity of mafic minerals in the FUV, meaning that immature features in the maria do not manifest as strongly in the original LAMP maps as they do in the OMAT map, leading to an oversubtraction.

from the background in the uncorrected off/on ratio map but have high OMAT, leading to the low values seen in the corrected off/on ratio and spectral slope maps (Figure 4). This suggests that we must be careful when interpreting results at some regions in the maria in these corrected maps or that a composition-dependent adjustment to the scale factor may be necessary; the highlands areas of the maps are free of such caveats. In the following paragraphs, we describe the process of making a composition-dependent adjustment to our corrected maps.

### 2.4. Composition-dependent Adjustment

Based on the previous finding that a number of immature high-Ti mare locations were spectrally similar to mature high-Ti mare regions in the FUV (Hendrix et al. 2016), we assume that the same is true throughout the entire maria (see Table S1 in supplemental information for justification of this assumption). In our final map, we therefore apply the full correction to the highlands and no correction to the maria. We acknowledge that while this assumption may not fully account for the impact of space weathering in the FUV at differing iron abundances, given the current dearth of knowledge on the subject, this was determined to be an adequate assumption.

For this final correction, we have chosen a 10 wt.% FeO abundance (based on the global FeO abundance map created from Lunar Prospector (LP) Gamma Ray Spectrometer (GRS) data; Lawrence et al. 2002) as the differentiating point between maria and highlands in our maps. In other words, we compared our LAMP maps with the FeO abundance map and performed the corrections from Equations (2)–(5) only on pixels with FeO $<$10 wt.%. We chose 10 wt.% as the cutoff because nearly all of the nearside mare basalt pixels are above this abundance threshold (Lawrence et al. 2002). It should be noted that some mare locations within South Pole Aitken (SPA) Basin have an FeO abundance below 10 wt.% and would have the correction applied to them. As previously stated, it is currently unknown to what extent space weathering affects the FUV spectral slope at moderate iron abundances such as those found in SPA, and we acknowledge that those regions may or may not be adjusted correctly. The final corrections (which replace the previous corrections and are applied to the original uncorrected LAMP maps) are as follows:

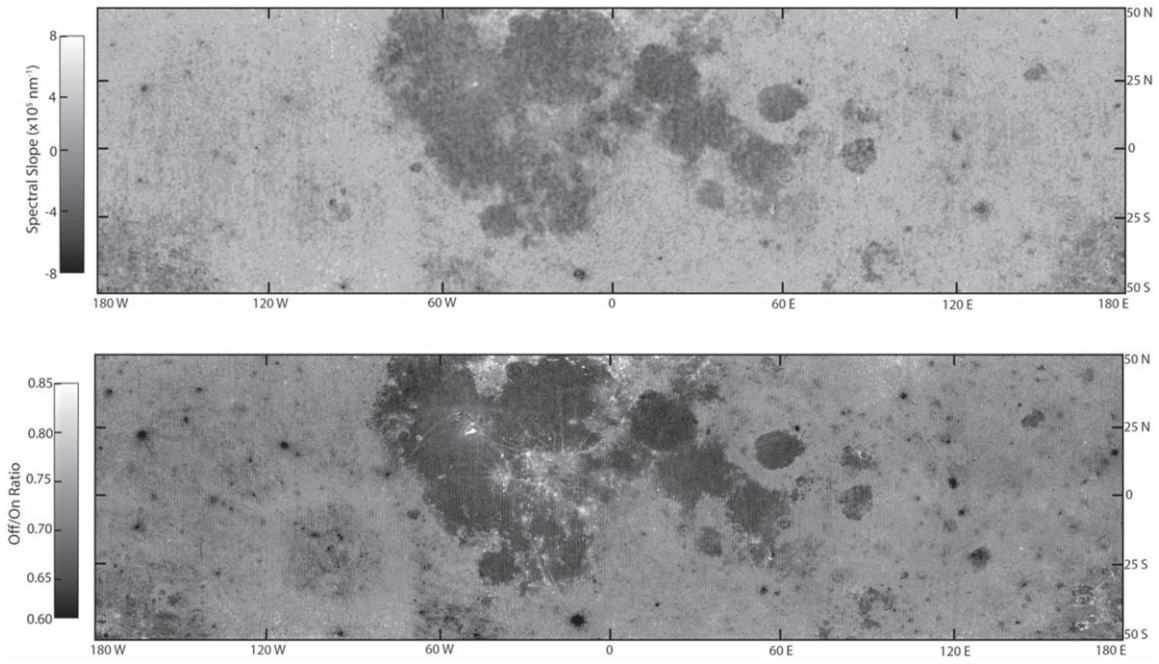


**Figure 5.** LAMP parameter maps after applying the OMAT correction. (Top) LAMP 170–187 nm spectral slope map and (bottom) off/on ratio map. After performing the correction, large-scale maturity-related features (e.g., crater rays) were removed from the map, revealing underlying features related to regolith composition.

Where FeO <10 wt.% and OMAT <0.2

$$ss_{\text{adjusted\_1}} = ss_{\text{orig}} - (8.5\text{x}10^{-4}\text{*OMAT}) + 1.4\text{x}10^{-4} \quad (6)$$

$$oo_{\text{adjusted\_1}} = oo_{\text{orig}} - (1.5\text{*OMAT}) + 0.235 \quad (7)$$

Where FeO <10 wt.% and OMAT >0.2

$$ss_{\text{adjusted\_2}} = ss_{\text{orig}} - (1.1\text{x}10^{-3}\text{*OMAT}) + 1.6\text{x}10^{-4} \quad (8)$$

$$oo_{\text{adjusted\_2}} = oo_{\text{orig}} - (2\text{*OMAT}) + 0.305 \quad (9)$$

While this final correction eliminated the artifacts due to overcorrection in the maria, we found that it introduced a separate complication. Ejecta from some large craters in the maria (which contain anorthositic material excavated from underneath the maria) appear to be undercorrected in the final maps. For example, ejecta from craters Copernicus and Kepler (as well as a section of a crater ray extending northwest from Tycho) are detected relative to the background maria in the corrected off/on ratio map. This is an effect that is difficult to avoid with the new method, as the FeO map is unable to fully distinguish some locations with anorthositic ejecta from the background mafic maria. Despite this issue, we maintain that Equations (6)–(9) provide an acceptable result on the global scale. For local area maps, more detailed derivations of the correction equations may provide a more accurate result than this general global correction.

## 3. Results

In the original uncorrected spectral slope and off/on ratio maps (Figure 1), rays originating from large young highlands craters (e.g., Tycho, Necho, and Giordano Bruno) display the reddest (most positive) spectral slopes and highest off/on ratios on the lunar surface. Smaller regions with redder spectral slopes and higher off/on ratios than the mature background are spread throughout the highlands and represent ejecta material from smaller highlands craters. The maria have bluer (less positive) slopes and lower off/on ratios than the highlands, demonstrating the compositional control on these parameters in addition to the clear maturity effects, as mentioned previously.

Figure 5 shows the adjusted spectral slope and off/on ratio maps after applying the corrections (described in Section 2). The red-sloped and high-ratio crater rays have been essentially removed, revealing features that are related to known differences in regolith composition from independent observations in other regions of the spectrum (e.g., young impact crater cavities). In Figure 6, we present the original and adjusted histograms for the 170–187 nm spectral slope and off/on ratio maps. In the original histograms (black lines), we see a tail of the distributions toward higher spectral slopes and off/on ratios, consisting primarily of immature highlands material from young rayed craters. After applying the maturity correction (red lines), the long tails of the distributions that were present in the original histograms (at high spectral slope and high ratio) have been largely removed.

The existence of artifacts/flaws in the various corrected FUV parameter maps demonstrates that, in some ways, regolith maturity manifests differently in the FUV than it does in the visible to near-IR, as measured by the OMAT parameter. An FUV-derived maturity parameter, i.e., one that is tied to Apollo-returned sample lab measurements that are not yet available, may therefore be necessary to enable the most accurate maturity correction to be performed with less subjectivity. Despite these issues, it is evident in Figure 5 that immature features have been largely removed after applying our maturity adjustment to the LAMP maps, and regolith composition can be interpreted more freely from maturity-related complications.

## 4. Discussion

### 4.1. Newly Revealed Features in Corrected LAMP Maps

Young impact crater cavities are a prominent feature in the corrected off/on ratio and spectral slope maps, appearing throughout the highlands as relatively dark (i.e., low ratio and

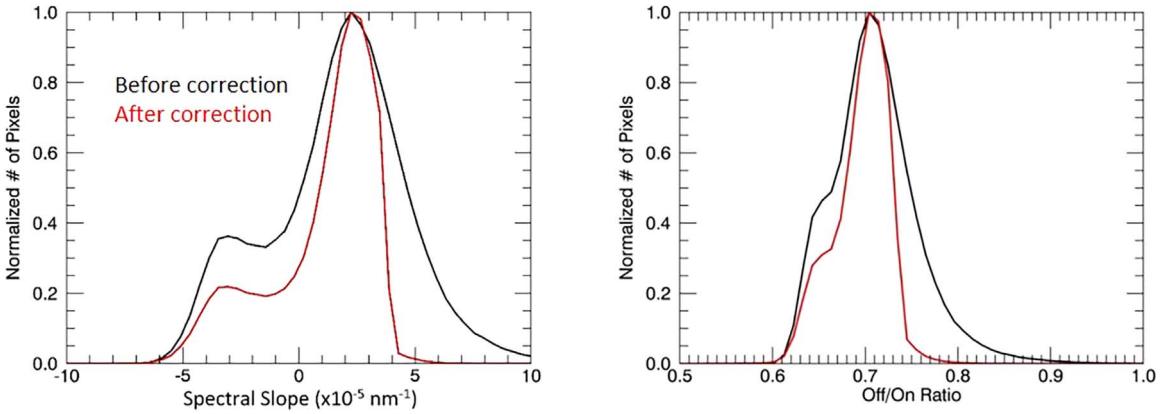


**Figure 6.** Histograms of the parameter maps before and after applying the OMAT correction. (Left) 170–187 nm spectral slope and (right) off/on ratio. In the corrected histograms (red lines), the long tail has been largely removed, displaying the removal of the maturity-related effects in the maps.

blue-sloped with respect to the background highlands) features. Previous studies have found evidence that the cavities (and surrounding halos) of many young impact craters contain a greater abundance of impact melt glass than the corresponding crater rays (Smrekar & Pieters 1985; Denevi et al. 2014). In the FUV, these melt-rich sites appear spectrally bluer due to either (a) the presence of the glassy silicate material, which is effectively opaque below ~200 nm (Kitamura et al. 2007), or (b) a greater abundance of pyroxene, which recent Moon Mineralogy Mapper results suggest exists at melt deposits as inclusions in a mixture with the glassy materials (Neish et al. 2021). Both of these would result in the UV absorption edge being shifted to longer wavelengths (Siegel 1974; Wagner et al. 1987), causing the observed decrease in off/on ratio and spectral slope relative to crystalline feldspathic material.

Another feature in the corrected off/on ratio map (that interestingly does not appear as strongly in the corrected spectral slope map) is Orientale Basin. The nonmare regions of the interior of the basin appear to have a slightly lower ratio than the extended ejecta, with a distinct boundary occurring near the basin outer ring. This suggests that the off/on ratio is detecting slight differences in mafic content or some other compositional effect between the inner ring and the outer extended ejecta. It is also possible, however, that the difference in ratio is a product of the correction (i.e., some compositional feature of the inner basin manifests more strongly in the OMAT map than it does in the off/on ratio map and is slightly overadjusted during the correction process). That would provide further evidence that regolith maturity manifests slightly differently in the FUV than in the IR for reasons that merit further investigation.

Recent results from Lucey et al. (2021), however, show a similar anomaly at Orientale after decorrelating CF and FeO. This suggests that the Orientale feature in the off/on ratio map is real, and that some compositional difference exists between the inner and outer basin ejecta. This highlights the fact that although differences exist between the CF and FUV parameters, similar compositional features manifest in both wavelength ranges. It is unclear why this feature occurs for Orientale and not for other locations, or why it is more evident in the off/on ratio map than in the spectral slope map, however.

### 4.2. Regolith Composition in the FUV

In order to identify how our FUV maps are affected by mineral composition, we compare our corrected LAMP spectral slope and off/on ratio maps with global mineral abundance maps created from a wide range of the electromagnetic spectrum, including LP GRS, Kaguya MI (near-IR), and LRO Diviner CF (mid-IR) data. We perform a pixel-by-pixel comparison of the spectral slope and off/on ratio with FeO abundance (Lawrence et al. 2002), plagioclase abundance (Lemelin et al. 2016), and thermal-IR CF (Greenhagen et al. 2010) maps and create scatter plots of each (Figure 7). We then calculate both Pearson and Spearman correlation coefficients for each of the scatter plots. Pearson correlation is an evaluation of the linear relationship between the two variables, and Spearman correlation is an evaluation of the monotonic relationship. We calculate both coefficients because the full scatter plots do not appear to be strictly linear but rather contain two separate clusters (the low-iron highlands and the high-iron maria). The full trends may therefore be better evaluated with the Spearman correlation. At moderate iron abundances, the relationships are more linear and may be better evaluated with the Pearson correlation.

What we see from the Spearman $R^2$ values in Figure 7 is that the FUV spectral slope displays better correlation with the mineral abundance maps than the off/on ratio does. At the highlands cluster (i.e., the lowest FeO and highest plagioclase abundances), there is an unexpected decrease in the mean spectral slope and off/on ratio with decreasing FeO/increasing plagioclase content.

While our LAMP parameters do not correlate well with the mineral abundance maps for regions with lower FeO content (<7 wt.%), they do correlate well for moderate- and high-iron regions and can be fit with a linear trend. For spectral slope versus FeO and plagioclase abundance, the Pearson $R^2$ correlation coefficients are 0.58 and 0.73, respectively, for pixels with an FeO abundance >7 wt.%. For the off/on ratio relative to FeO and plagioclase abundance, the Pearson $R^2$ values are 0.34 and 0.53, respectively, for the same pixels. To understand the reason for this good correlation in the moderate- to high-iron regions, we must consider the mechanism behind the bluing effect of mafic minerals in the FUV.

The spectra of soils with low mafic content (e.g., the lunar highlands) have a higher spectral slope, <170 nm, than soils with greater mafic content, a result of the plagioclase UV absorption edge extending into the FUV (Wagner et al. 1987). The location of this absorption edge marks the volume scattering–to–surface scattering transition point, and the sharpness of the edge is degraded by FeO charge-transfer

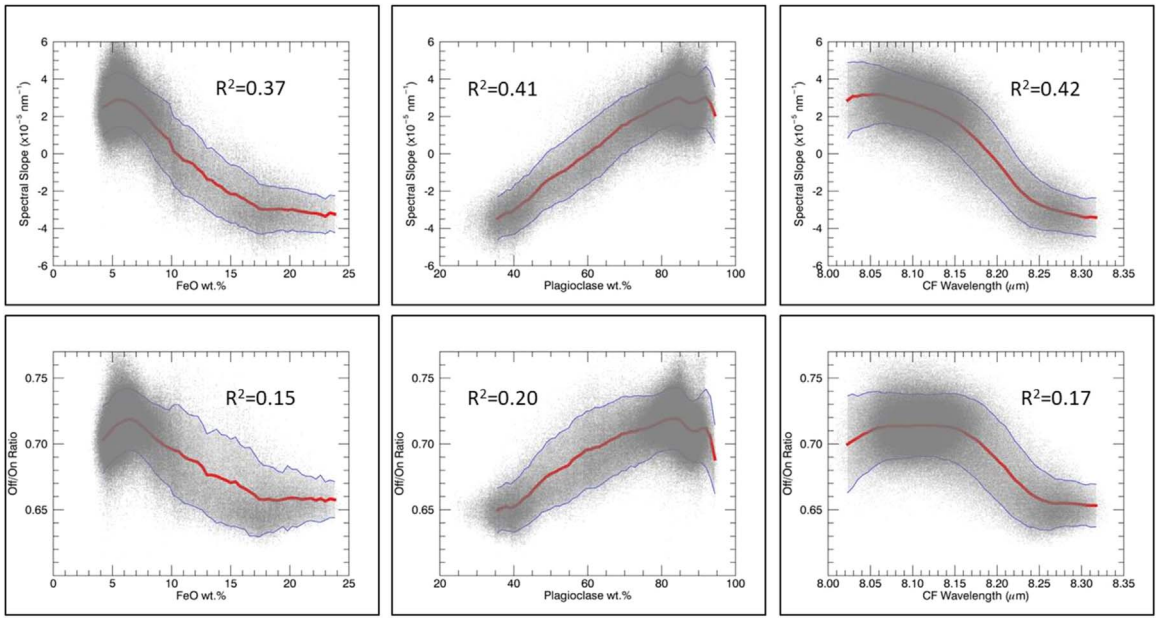


**Figure 7.** Comparison with mineralogy maps. The scatter plots compare the corrected (top row) 170–187 nm spectral slope and (bottom row) off/on ratio with mineral abundance maps derived from other data sets. Mean and standard deviation values are represented by red and blue lines, respectively, and $R^2$ values represent Spearman correlation coefficients. The spectral slope shows better correlation with the mineralogy maps than the off/on ratio does. Additionally, the LAMP parameters generally show better correlation with the mineral abundance maps for regions with moderate–high iron content (FeO >7%) than for regions with low iron content.

absorption bands that become broader with an increasing abundance of mafic minerals (Cloutis et al. 2008). At wavelengths longward of the transition point, volume scattering is dominant due to the higher penetration depth of light. At wavelengths shortward of the transition point (i.e., most of the FUV), the penetration depth is shallow, surface scattering is dominant, and the reflectance of a mineral depends on its index of refraction (Henry et al. 1976).

The volume scattering–to–surface scattering transition is marked by a minimum in reflectance, and for Fe-poor anorthositic material, this minimum can occur within the FUV (e.g., at fresh highlands ejecta; Hendrix et al. 2016; Byron et al. 2020a). With increasing Fe abundance, this minimum in reflectance is shifted toward longer wavelengths (Cloutis et al. 2008). In the more mafic maria, for example, LAMP may not see the transition point, as it would occur at longer wavelengths beyond the LAMP bandpass. However, the good correlation between the LAMP parameters and Fe abundance for moderate–high Fe regions indicates that they are still affected by the changes despite the transition point occurring outside of the LAMP wavelength range. The likely cause of this is the broadening of the absorption band that accompanies the shift in band minimum at increasing Fe abundance (Cloutis et al. 2008). Although LAMP may not see the volume scattering–to–surface scattering spectral transition point for the more mafic areas of the lunar surface, the effects of broadening the absorption band are likely to stretch into the FUV and have an impact on the spectral slope and off/on ratio. Furthermore, the slightly better correlations for the 170–187 nm spectral slope suggest that it is more sensitive to these changes than the off/on ratio, and that the spectral slope may be the best tool for future use in FUV compositional studies.

In the highlands, space weathering acts to degrade the plagioclase FUV absorption edge (i.e., lower the reflectance and shift the absorption shoulder to longer wavelengths) through the addition of SMFe particles to the rims of the plagioclase grains. This process is similar to that which causes the negative spectral slopes in the maria, but the lower availability of iron in the highlands prevents even fully mature highlands regolith from reaching a spectral slope as blue as that of the maria (Hendrix et al. 2016). By performing the maturity correction, we have artificially degraded the absorption edge (and decreased the spectral slope) to the theoretical maximum degree in the highlands. This would explain the lack of any significant compositional (FeO, plagioclase, and CF) correlations for these low-iron regions.

### 4.3. LAMP Wavelength/Sensing Depth and Composition

One thing to consider when attempting mineralogical studies with LAMP is the shallow sensing depth of FUV photons compared to the longer wavelengths measured with instruments like Kaguya MI and Diviner. LAMP is not necessarily sensing the same mineral and grain properties as these other instruments with deeper sensing depths. For example, the Kaguya MI data used to derive the plagioclase map (Lemelin et al. 2016) range from ∼0.4 to 1.5 μm. So, while LAMP is sensing only the top ∼100 nm of the rim of a regolith grain, the longer-wavelength instruments are probing deeper into the same grain.

Similarly, Diviner CF measurements in the thermal IR represent the peak emissivity of a mineral spectrum, which is correlated with the location of the fundamental vibrational band. The charge-transfer absorption bands that LAMP observes in the FUV, however, are caused by electronic transitions and would be unaffected by the fundamental vibrational transitions. So, while LAMP does seem to be sensitive to regolith silicate abundance (as evidenced by the good correlation with the Diviner CF location), it is sensitive in a different way than for the CF diagnostic technique. Further study is needed to fully understand the ways that the FUV reflectance is affected by mineral composition, and these corrected maps provide a crucial first step toward that understanding.

## 5. Conclusion

We have performed a correction to LAMP 170–187 nm spectral slope and off/on ratio maps for optical maturity founded on the OMAT parameter derived from Kaguya MI data. The goal of this correction was to enable surface composition to be analyzed free from the prevalent effects of regolith maturity in FUV maps. Large-scale immaturity features (e.g., crater rays) were successfully removed from the LAMP global maps, revealing features related to regolith composition. However, some regions of the maria contained artifacts that were introduced during the map correction process, suggesting that regolith maturity manifests differently in the FUV versus the near-IR. In order to limit the introduction of such artifacts to the maps, we performed the maturity correction only on pixels with an FeO abundance below 10 wt.% (derived from LP GRS data). This successfully removed the artifacts from the corrected maps; however, it may have led to undercorrections at some locations in the maria (e.g., a crater ray extending northwest from Tycho into the maria).

Despite differences in wavelength and sensing depth between the FUV and the IR, the corrected LAMP parameters show good correlation with FeO, plagioclase, and CF parameter maps for moderate- to high-iron regions. This indicates a sensitivity in the LAMP data to changes in mineral abundance. We additionally found that of our two LAMP parameter maps, the spectral slope showed better correlations with the mineral abundance maps, suggesting that the spectral slope may be the better tool for use in FUV compositional studies. These maps demonstrate the effectiveness of compositional mapping using FUV measurements, and further analyses of specific locations with these new maps will enable us to more fully understand the effects of lunar regolith composition in the FUV.

This work was funded by the Lunar Reconnaissance Orbiter (LRO) Lyman Alpha Mapping Project (LAMP) under NASA contract NNG05EC87C. All LAMP data used in this study are available at the Planetary Data System Cartography and Imaging Sciences Node (https://pds-imaging.jpl.nasa.gov/volumes/lro.html). This work was done as a private venture and not in the author's capacity as an employee of the Jet Propulsion Laboratory, California Institute of Technology.

## Appendix

A wide range of factors and offsets were tested before settling on those listed in Equations (2) and (3). An example of two tests for the off/on ratio correction are shown in Figure A1. In test correction 1, the higher off/on ratio tail remains undercorrected. Conversely, in test correction 2, the lower off/on ratio values have been overcorrected. The corrections listed in Section 2 represent the corrections that provided the best results.

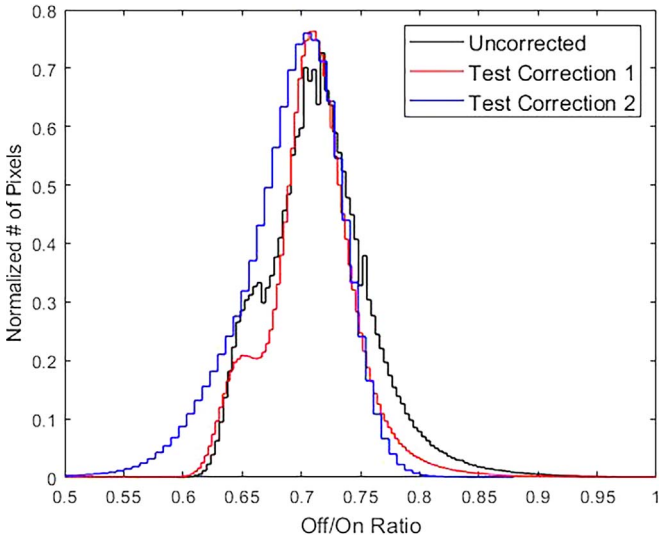


**Figure A1.** Histograms of test factor/offset corrections. Test Correction 1 represents an undercorrection, and Test Correction 2 represents an overcorrection.

Test Correction 1: $oo_{\text{adjusted\_1}} = oo_{\text{orig}} - (1^{*}\text{OMAT}) + 0.155$

Test Correction 2: $oo_{\text{adjusted\_1}} = oo_{\text{orig}} - (2.5^{*}\text{OMAT}) + 0.385$

After applying the initial best-fit corrections (Equations (2) and (3)) to the spectral slope and off/on ratio maps, we found that some portions of the ejecta from the largest young craters (e.g., Tycho, Giordano Bruno) were slightly undercorrected and still apparent in the corrected maps (Figure A2). After applying a further correction on pixels with OMAT >0.2 (listed in Equations (4) and (5)), these undercorrected features were fully normalized.

Previous work by Hendrix et al. (2016) found that fresh high-Ti mare craters (locations 9–14 in Table 1 of Denevi et al. 2014) had a similar spectral slope to a mature high-Ti mare location. Based on this finding, it could be assumed that a maturity correction would not be necessary for the maria in our LAMP maps. In order to further justify not performing a correction to mare locations (as in our final corrections of Equations (6)–(9)), we have calculated the off/on ratio at a number of fresh craters in the maria and the highlands (based on Table 1 of Denevi et al. 2014). The results in Tables A1 and A2 show that fresh craters in both high-Ti (mean = 0.664) and low-Ti (0.651) mare locations have similar off/on ratios to high-Ti (0.0643) and low-Ti (0.0661) mature maria, while both low-Fe (0.918) and moderate-Fe (0.859) fresh craters in the highlands have much higher off/on ratios than the low-Fe (0.703) and moderate-Fe (0.726) mature highlands. The main conclusion from this is that, because maturity does not seem to affect the off/on ratio or spectral slope for either high- or low-Ti mare locations, any maturity correction for the maria would be inappropriate.

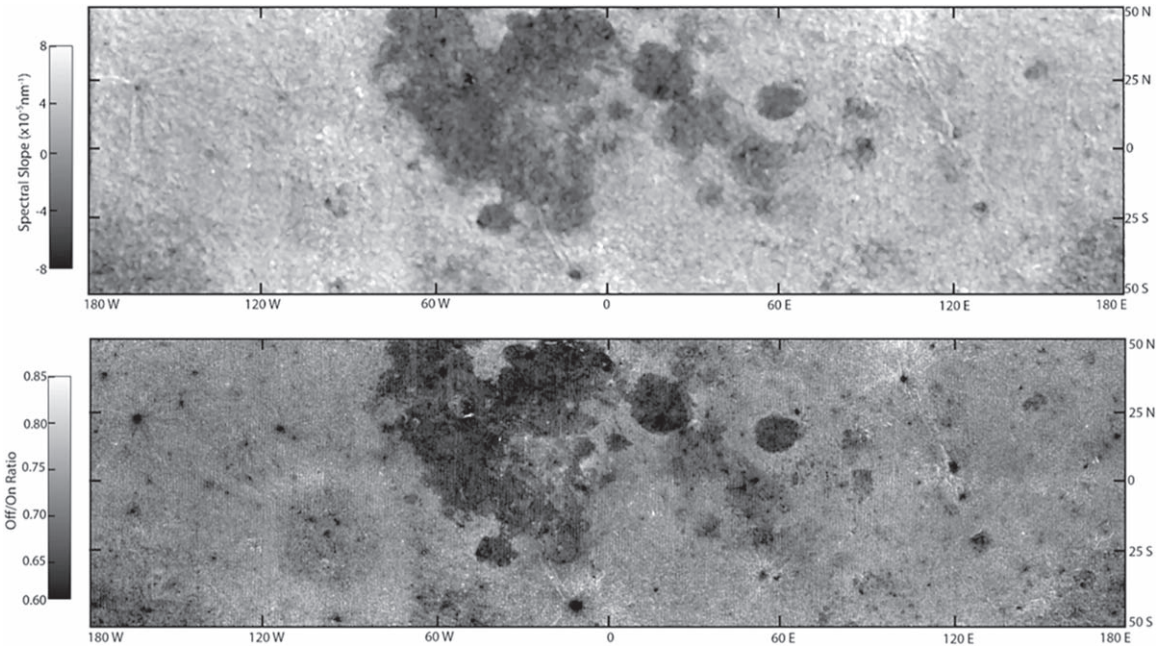


**Figure A2.** Intermediate step corrected maps. (Top) LAMP 170–187 nm spectral slope map and (bottom) off/on ratio map after applying Equations (2) and (3). Further increasing the factor values results in a slight overcorrection throughout most of the highlands. Portions of the largest crater rays (from Tycho, Necho, and Giordano Bruno, for example) are still visible, however. A separate correction is necessary for these pixels.

**Table A1**
Selected Fresh Craters from Denevi et al. (2014)

| Location No. | Type | Latitude | Longitude | Off/on Ratio |
|---|---|---|---|---|
| 1 | Low-Ti mare | 19.76 | 24.44 | 0.659 |
| 2 | Low-Ti mare | 19.71 | 22.53 | 0.635 |
| 3 | Low-Ti mare | 21.17 | 23.68 | 0.657 |
| 4 | Low-Ti mare | 27.79 | 11.79 | 0.667 |
| 5 | Low-Ti mare | 47.80 | 290.97 | 0.638 |
| 6 | Low-Ti mare | 40.83 | 289.77 | 0.610 |
| 7 | Low-Ti mare | 28.55 | 325.76 | 0.665 |
| 8 | Low-Ti mare | 32.07 | 328.12 | 0.673 |
| 9 | High-Ti mare | 9.88 | 311.66 | 0.682 |
| 10 | High-Ti mare | 13.11 | 24.50 | 0.652 |
| 11 | High-Ti mare | 40.09 | 333.79 | 0.645 |
| 12 | High-Ti mare | 10.89 | 314.47 | 0.689 |
| 13 | High-Ti mare | −4.98 | 324.79 | 0.654 |
| 14 | Mod-Fe highland | 9.29 | 250.02 | 0.830 |
| 15 | Mod-Fe highland | −41.33 | 188.29 | 0.832 |
| 16 | Mod-Fe highland | 46.60 | 49.74 | 0.984 |
| 17 | Mod-Fe highland | 4.50 | 101.06 | 0.886 |
| 18 | Mod-Fe highland | −19.33 | 302.75 | 0.764 |
| 19 | Low-Fe highland | 3.47 | 259.63 | 0.964 |
| 20 | Low-Fe highland | −5.03 | 255.58 | 0.834 |
| 21 | Low-Fe highland | 7.84 | 182.96 | 0.833 |
| 22 | Low-Fe highland | 17.60 | 182.00 | 0.822 |
| 23 | Low-Fe highland | 19.40 | 166.69 | 1.134 |
| 24 | Low-Fe highland | 18.32 | 202.68 | 0.920 |

**Table A2**
Selected Mature Locations from Denevi et al. (2014)

| Type | Latitude | Longitude | Off/on Ratio |
|---|---|---|---|
| Mature low-Ti mare | 32.12 | 328.65 | 0.643 |
| Mature high-Ti mare | 11.17 | 314.44 | 0.661 |
| Mature mod-Fe highlands | −19.64 | 302.89 | 0.726 |
| Mature low-Fe highlands | 27.12 | 169.81 | 0.703 |

## ORCID iDs

Benjamin D. Byron https://orcid.org/0000-0003-4435-0347
Kurt D. Retherford https://orcid.org/0000-0001-9470-150X
Elizabeth Czajka https://orcid.org/0000-0003-1874-4158
Joshua T. S. Cahill https://orcid.org/0000-0001-6874-5533
Amanda R. Hendrix https://orcid.org/0000-0002-0435-8224
Thomas K. Greathouse https://orcid.org/0000-0001-6613-5731

## References

Byron, B. D., Retherford, K. D., Greathouse, T. K., et al. 2019, JGRE, 124, 823
Byron, B. D., Retherford, K. D., Greathouse, T. K., et al. 2020a, JGRE, 125, e06269
Byron, B. D., Retherford, K. D., Greathouse, T. K., Cahill, J. T. S., & Hendrix, A. R. 2020b, LPSC, 51, 2771
Cahill, J. T., Wirth, A. A., Hendrix, A. R., et al. 2019, JGRE, 124, 294
Cloutis, E. A., McCormack, K. A., Bell III, J. F., et al. 2008, Icar, 197, 321
Davis, M. W., Greathouse, T. K., Kaufmann, D. E., Retherford, K. D., & Versteeg, M. H. 2017, Proc. SPIE, 10397, 1039717
Denevi, B. W., Robinson, M. S., Boyd, et al. 2014, JGRE, 119, 976
Gladstone, G. R., Retherford, K. D., Egan, A. F., et al. 2012, JGRE, 117, E00H04
Gladstone, G. R., Stern, S. A., Retherford, K. D., et al. 2010, SSRv, 150, 161
Greenhagen, B. T., Lucey, P. G., Wyatt, M. B., et al. 2010, Sci, 329, 1507
Hendrix, A. R., Greathouse, T. K., Retherford, K. D., et al. 2016, Icar, 273, 68
Hendrix, A. R., Retherford, K. D., Gladstone, G. R., et al. 2012, JGRE, 117, E12001
Hendrix, A. R., & Vilas, F. 2006, AJ, 132, 1396
Henry, R. C., Fastie, W. G., Lucke, R. L., & Hapke, B. W. 1976, Moon, 15, 51
Kitamura, R., Pilon, L., & Jonasz, M. 2007, ApOpt, 46, 8118
Lawrence, D. J., Feldman, W. C., Elphic, R. C., et al. 2002, JGRE, 107, 5130
Lemelin, M., Lucey, P. G., Gaddis, L. R., Hare, T., & Ohtake, M. 2016, LPSC, 47, 2994
Liu, Y., Retherford, K. D., Greathouse, T. K., et al. 2018, JGRE, 123, 2550
Lucey, P. G., Blewett, D. T., Taylor, G. J., & Hawke, B. R. 2000, JGRE, 105, 20377
Lucey, P. G., Greenhagen, B. T., Donaldson Hanna, K. L., et al. 2021, JGRE, 126, e06777

Lucey, P. G., Greenhagen, B. T., Song, E., et al. 2017, Icar, 283, 343
Mandt, K. E., Greathouse, T. K., Retherford, K. D., et al. 2016, Icar, 273, 114
Neish, C. D., Cannon, K. M., Tornabene, L. L., et al. 2021, Icar, 361, 114392
Noble, S. K., Pieters, C. M., & Keller, L. P. 2007, Icar, 192, 629
Pieters, C. M., Taylor, L. A., Noble, S. K., et al. 2000, M&PS, 35, 1101
Siegel Jr., G. H. 1974, JNCS, 13, 372
Smrekar, S., & Pieters, C. M. 1985, Icar, 63, 442
Wagner, J. K., Hapke, B. W., & Wells, E. N. 1987, Icar, 69, 14